

**TiAlN based nanoscale multilayer coatings designed to adapt their tribological properties at elevated temperatures**

HOVSEPIAN, Papken <<http://orcid.org/0000-0002-1047-0407>>, LEWIS, D. B., LUO, Q. <<http://orcid.org/0000-0003-4102-2129>> and MUNZ, W. D.

Available from Sheffield Hallam University Research Archive (SHURA) at:

<https://shura.shu.ac.uk/585/>

---

This document is the Accepted Version [AM]

**Citation:**

HOVSEPIAN, Papken, LEWIS, D. B., LUO, Q. and MUNZ, W. D. (2005). TiAlN based nanoscale multilayer coatings designed to adapt their tribological properties at elevated temperatures. Thin solid films, 1-2. [Article]

---

**Copyright and re-use policy**

See <http://shura.shu.ac.uk/information.html>

# **TiAlN based nanoscale multilayer coatings designed to adapt their tribological properties at elevated temperatures**

P. Eh. Hovsepián<sup>1</sup>, D. B. Lewis<sup>1</sup>, Q. Luo<sup>1</sup>, W. -D. Münz<sup>1</sup>, P. H. Mayrhofer<sup>2</sup>, C. Mitterer<sup>2</sup>, Z. Zhou<sup>3</sup>, W. M. Rainforth<sup>3</sup>

<sup>1</sup> Materials and Engineering Research Institute, Sheffield Hallam University, Howard Street, Sheffield, S1 1WB, UK,

<sup>2</sup> Department of Physical Metallurgy and Materials Testing, University of Leoben, Franz-Josef-Strasse 18, A-8700, Leoben, Austria,

<sup>3</sup> Department of Engineering Materials, University of Sheffield, Sheffield, S1 3JD, UK

## **Abstract**

The addition of properly selected elements, coupled in nanoscale multilayer structures can further enhance the properties of TiAlN coatings and bring new high performance. The incorporation of Y in the nanoscale pseudo-superlattice TiAlCrN/TiAlYN with typical period of 1.7 nm not only improves the oxidation resistance but also effectively reduces the coefficient of friction of the coating from 0.9 to 0.65 at temperatures in the range of 850 - 950 °C. The adaptation of the tribological properties occurs as a result of the preferential migration of the Y to the column boundaries. TiAlN/VN superlattice can achieve another self-adaptation process. During friction the coatings adapt themselves to the combined thermal and mechanical wear by the formation of highly lubricious vanadium-oxides due to high flash temperatures at the asperity contacts on the surface. The integrity of the bulk of the coating is retained, leading to exceptionally low, for superhard coatings, friction coefficient of 0.5 and a wear coefficient of  $2 \times 10^{-17} \text{ m}^3 \cdot \text{N}^{-1} \cdot \text{m}^{-1}$ . The coatings have been deposited by the combined steered cathodic arc unbalanced magnetron sputtering method.

## 1 Introduction

The demand for high performance physical vapor deposition (PVD) coatings to resist degradation in severe environments, endurance of extremely high thermo-mechanical loads in particular is ever increasing. Additionally, in recent years, a demand for a new generation of coatings capable to adapt their surface or bulk properties to these severe conditions has emerged. In an attempt to combat wear in an environment with a variable humidity a super-tough wear resistant WC/diamond-like-carbon/WS<sub>2</sub> coating with “chameleon” surface adaptation has been developed [1]. The adaptation effect lies in the synergy of smart material and structure selection processes and has been proved for low temperatures. The combination of nanocrystalline grains and amorphous matrix initially developed for super-hardness and improved toughness [2 – 4] has shown also potential for self-adaptation in specific conditions. In the medium temperature range up to 500 °C, yttrium-stabilized -zirconia/Au utilising composite (nanocrystalline / amorphous) structures have shown consistently low friction coefficient due to the microstructure adaptive changes and formation of lubricating Au transfer films [5]. Recent research on the effect of the age hardening, in Ti<sub>1-x</sub>Al<sub>x</sub>N has considered the effect as self adaptation mechanism contributing towards maintaining high wear resistance at elevated temperatures (up to 1000 °C). It has been demonstrated that in this temperature range, Ti<sub>1-x</sub>Al<sub>x</sub>N coatings undergo spinodal decomposition into coherent face-centre-cubic (fcc) structured AlN and fcc-TiN nanometer-size domains. This transformation generates an increase in hardness due to coherency stresses and therefore enhances the wear resistance at elevated temperatures [6, 7].

The requirement for high temperature stability involves several key applications, which gain increasing importance in modern technology, such as dry high speed machining [8], machining of “sticky” alloys used in aerospace and automotive industries [9] as well as protection of high duty components in aero and automotive engines manufactured from prone to oxidation materials [10]. In all the above mentioned applications, the Ti<sub>1-x</sub>Al<sub>x</sub>N coating

family has been recognised as successful alternative, due to their excellent resistance to micro-abrasive wear and to high temperature oxidation up to 750 °C. The remarkable high temperature stability of these coatings has been attributed to the formation of highly protective double layer oxide scale including a very dense Al<sub>2</sub>O<sub>3</sub> top layer [11]. Further enhancement of the functional properties of these coatings has been achieved by incorporating of active elements to Ti<sub>1-x</sub>Al<sub>x</sub>N, such as Cr and Y [12]. Several mechanisms have been proposed to explain the improved protective nature of the scale, due to the incorporation of Y, such as improvement of the mechanical adherence of the Al<sub>2</sub>O<sub>3</sub> scale, reduction of the scale growth rate, grain refinement, and “plugging” diffusion paths via segregation at the grain boundaries [13, 14].

To address specific applications however, the properties of the Ti<sub>1-x</sub>Al<sub>x</sub>N based coatings can also be tailored successfully by structural design. Utilising the nanoscale multilayer, superlattice structures and combining selected coating materials allows extremely high hardness, > 40 GPa to be achieved [15, 16]. Together with the structure, the compressive stress will also play an important role in hardness enhancement. This factor can be easily controlled by the applied bias voltage during the coating deposition process [16]. Layering with VN in TiAlN/VN superlattice structures in addition to the super-hardness however, brings a unique tribological behaviour, due to the formation of a low melting point highly lubricious V<sub>2</sub>O<sub>5</sub>, during sliding [16 – 18]. The exceptionally low coefficient of friction and wear rates, achieved by this approach bring into consideration another adaptation mechanism, which can be described as a compositionally regulated tribo-oxidation process, taking place under the conditions of the tribological contact.

This paper summarises the experience gained in the development and exploitation of two TiAlN based nanoscale multilayer structured PVD coatings namely TiAlCrN/TiAlYN and TiAlN/VN. The ability of the coatings to self organise and adapt to the environment utilising

segregation mechanisms triggered by the exposure to high temperatures as well as by the formation of friction reducing liquefied tribofilms of  $V_2O_5$  will be described.

## **2 Technological aspects in deposition of nanoscale multilayer, superlattice structured TiAlCrN/TiAlYN and TiAlN/VN coatings.**

TiAlCrN/TiAlYN and TiAlN/VN nanoscale multilayer coatings have been produced in a computer- controlled Hauzer HTC 1000-4 coater, utilising the combined cathodic arc/unbalanced sputtering technique, known also as Arc-Bond-Sputtering (ABS) technique [19, 20]. The coater comprises four linear dual- purpose cathodes, which can be operated either in steered arc or unbalanced magnetron sputtering mode. Fig. 1a schematically outlines the cross-section of the system, with a typical target arrangement used for deposition of TiAlCrN/TiAlYN. The key advantage of the ABS approach is the utilization of a metal ion pre-treatment (metal ion etching) of the substrate material prior to the coating deposition step, which results in excellent coating adhesion. During the surface pre-treatment step, typically 20 min long, metal ions generated from an arc discharge sustained on one of the targets are accelerated towards the substrate due to the applied high bias voltage ( $U_b = -1200$  V). In the case of  $Cr^+$  ion etching, high substrate current densities of  $20 \text{ A}\cdot\text{m}^{-2}$  have been measured by flat Langmuir probe facing the target [21]. Under these conditions, the energy of the arriving gas-metal ions is sufficient to produce surface etching, low energy metal ion implantation and to promote local epitaxial growth of the coating [21, 22].  $Cr^+$  ion etching is used to treat the surface prior to deposition of TiAlCrN/TiAlYN, whereas  $V^+$  etching is employed in the case of TiAlN/VN coating. The macro particles emitted from the arc discharge produce growth defects in the coating [23] without disrupting the nanoscale multilayer structure of the coating. However, the growth defects reduce locally the oxidation resistance of the coating due to their under-dense structure [24]. Previous work has shown that the adhesion is of paramount importance in applications such as dry high speed milling where the tools are subjected to interrupted reciprocating impact loads. In this application the tool lifetime is

proportional to the critical load values in scratch testing [20]. Furthermore, depending on the deposition conditions both nanoscale multilayer coatings exhibit relatively high compressive residual stress, up to -7 GPa, which can only be maintained by strong adhesion. This problem is further addressed by deposition of stress reduced 0.2 – 0.3  $\mu\text{m}$  thick base layer of TiAlCrN or VN prior to the deposition of the TiAlCrN/TiAlYN or TiAlN/VN coating, respectively.

The HTC 1000-4 system is equipped with a threefold planetary rotating table, which in combination with the multi target arrangement utilising linear sources allows straightforward deposition of nanoscale multilayer coatings. High deposition rates (typically of 1  $\mu\text{m}$  per hour) are achieved by avoiding complicated installations, such as shielding and shuttering. The coatings are deposited by reactive unbalanced magnetron sputtering in a common Ar + N<sub>2</sub> atmosphere at temperature of 450 °C. The deposition of TiAlCrN/TiAlYN coatings requires one Cr (99.8 at.%), two Ti<sub>0.5</sub>Al<sub>0.5</sub> and one Ti<sub>0.48</sub>Al<sub>0.48</sub>Y<sub>0.04</sub> targets. The incorporation of the Y in one target only is deliberate, to achieve layered distribution of Y in the coating. This target will usually be installed between the two TiAl targets as shown in Fig. 1a. The individual layer thickness in the nanoscale multilayer coatings is controlled precisely by the power dissipated on the targets, sample rotation speed, applied bias voltage and the composition of the reactive atmosphere, controlled in total pressure controlled mode ( $\Delta p_{\text{Ar}} + \Delta p_{\text{N}_2} = \text{constant}$ ). To deposit TiAlN/VN superlattice structured coatings, schematically shown in Fig. 1b, two pairs of adjacent Ti<sub>0.5</sub>Al<sub>0.5</sub> and V targets (99.8% pure) have been used. All the coatings were deposited on mirror polished M2 high speed steel, hardened to HRC 63, for adhesion and tribological characterisation, on cemented carbides for high temperature tribotest, and on AISI 316 stainless steel for structural characterisation. Two-flute ball nosed cemented carbide end mills, 8 mm in diameter, have been also coated for cutting tests. Prior to the coating, all substrates were cleaned in an automated cleaning line, comprising a series of ultrasonically agitated aqueous alkali solutions and deionised water baths and a vacuum dryer.

### 3 Thermal behaviour of the nanoscale (pseudo-superlattice) structured

#### TiAlCrN/TiAlYN coating

Compared to previous generation of TiAlN coatings, TiAlCrN/TiAlYN exhibit significantly higher resistance to oxidation and to abrasive wear. It has been reported that the onset of rapid oxidation of TiAlN in thermo-gravimetric tests has been increased from 750 °C to 850 °C and further to 950 °C by the incorporation in the coating of 3 at.% Cr and 2 at.% Y respectively [25, 26]. It has been shown in [25] that the incorporation of a large and therefore relatively immobile Y atom (atomic radius 0.18 nm) leads to repeated re-nucleation in the growing film, resulting in a much finer grain size (typically in the range of 5 – 10) compared to that of the TiAlN and a near equi-axed grain morphology. The incorporation of Y in TiAlCrN in a layered manner has been found to be from a key importance for its efficiency to enhance both the oxidation resistance as well as the high temperature tribological behavior of the coating. The Y containing layers are separated at a distance of  $\Delta = 1.7$  nm to form a pseudo superlattice TiAlCrN/TiAlYN coating. The term “pseudo superlattice” is used here mainly to emphasise the layered incorporation of the Y and the single phase structure of the coating. Due to the small bilayer thickness however, the typical for the “true” superlattices, ( $\Delta = \underline{3 – 5}$  nm) hardness enhancement (the superlattice effect, [27] ) can not be realised. The typical hardness values for this coating are in the range of  $HK_{0.025} = 27$  GPa. The incorporation of Y leads to accumulation of high residual stress, typically of -7 GPa. Therefore, in addition to the  $Cr^+$  metal ion etching, a 300 nm thick Y free TiAlCrN base layer of low stress (-3.2 GPa) is deposited with a main role to provide a smooth transition in stress and hardness from the substrate material to the coating to achieve superior adhesion. This strategy proved to be efficient as critical load values of  $L_c = 60$  N have been measured in scratch adhesion test when the coating is deposited on hardened high speed steel substrate [26].

To further understand the effect of Y on the thermal stability and oxidation behaviour of TiAlN based coatings, two combinations of superlattice structured coatings were investigated,

in which TiAlYN and CrN were selected as a second partner material. It has been anticipated that the thermal stability of the nanoscale multilayer structures will be additionally enhanced due to the higher activation energies for diffusion and oxidation compared to the monolithically grown structures [28]. Thermo-gravimetric analysis carried out in long duration (up to 1000 h) iso-thermal tests in air at 750 °C showed that both TiAlCrN/TiAlYN and TiAlN/CrN coatings are highly oxidation resistant. In this test however, the Y free coating exhibited accelerated mass gain with increasing exposure time reaching mass gain in the end of the test of  $1.2 \times 10^{-3} \text{ g}\cdot\text{cm}^{-2}$  compared to  $8 \times 10^{-4} \text{ g}\cdot\text{cm}^{-2}$  measured for the TiAlCrN/TiAlYN coating. It has been found through detailed cross-sectional microstructure examination that, the accelerated oxidation in the TiAlN/CrN coating was attributed to internal oxidation of the sub-dense columnar structure. After the long term iso-thermal process, no multilayer fringes could be seen in the TiAlN/CrN indicative of homogenization of the as-deposited TiAlN/CrN multilayer. Additionally, the coating exhibited numerous places of inter-column porosity, Fig. 2a. The openings in the structure between the columns can be attributed to reduction of the coating volume and development of tensile stress due to annealing-out of voids or vacancies (Schottky defects) during the high temperature treatment [29]. The cross-sectional transmission electron microscopy (TEM) analysis also revealed a multitude of sites of internal oxidation in the bulk of the TiAlN/CrN coating associated mainly with the inter-column porosity as the porous inter-column areas worked as tunnels for the inward oxygen diffusion. In the monolithically grown TiAlCrN base layer as expected, the internal oxidation and the structural porosity were even more pronounced and severe, Figure 2b.

In contrast, the incorporation of Y in the TiAlCrN/TiAlYN coating resulted in fully dense columns and dense column boundaries and no evidence for internal oxidation was found. Fig. 3 shows a cross-sectional TEM micrograph of the iso-thermal treated TiAlCrN/TiAlYN illustrating the overall structure of the coating including the surface, the bulk and the base

layer regions. On the surface of the TiAlCrN/TiAlYN coating a 1.6  $\mu\text{m}$  thick continuous oxide scale had been formed followed by a transition region. The top part of the oxide scale appeared dense, fully crystallised and rich in aluminium, which provided a barrier to the inward diffusion of oxygen thus contributing to slower oxidation rate. In the nitride-oxide transition region, the TiAlCrN/TiAlYN coating was decomposed by progressive release of nitrogen followed by the formation of amorphous-like multicomponent oxide.

The higher density in aluminium- rich top oxide layer undoubtedly provides better protection against the environmental attack. However this can not explain the high density of the bulk of the coating retained after the long term exposure to high temperatures. This special behaviour can be attributed to the segregation of the Y into the grain boundaries [25]. Fig. 4 shows a scanning TEM (STEM) energy dispersive X-ray analysis (EDX) elemental map demonstrating this unique behaviour [30]. The preferential diffusion of Y to potentially sub-dense regions, such as grain boundaries is predetermined by the large size of the Y atom and the kinetics of the recovery process of thermodynamically unstable phases, taking place during annealing. It has been reported that the thermal stability of defects in the PVD coatings strongly depends on the biaxial stress in the as deposited state [31]. The introduction of 2% Y in the TiAlN leads to a large lattice distortion, increasing the lattice parameter  $a_0$  from 0.418 nm for the Y-free coating to 0.424 nm, which results in accumulation of high compressive stress, -7 GPa. The accumulated stress in this case, will provide the driving force in the annealing process, whereas the recovery in the material will occur through the mechanism of the yttrium segregation at the grain boundaries. This mechanism can be classified as a self-healing and self- adapting mechanism. The segregation mechanism opposes and prevents opening of large voids due to material volume reduction in the coating, by supplying Y atoms at the vulnerable sites and therefore retaining the coating integrity. No such self-healing mechanism operates in the Y-free TiAlCrN base layer, therefore a significant structure changes, mainly pronounced inter-column porosity was observed, Fig. 3. The formation of

this sub-dense structure has allowed significant outward diffusion of substrate elements into the base layer, which has been demonstrated by quantitative TEM-EDX analysis and scanning TEM-EDX elemental mapping [10, 30]. In contrast no sign of inward and outward diffusion of oxygen or substrate material elements has been found in the densified bulk of the coating. Further evidence on the adaptation and self-healing effect can be found in investigating the high temperature wear properties of TiAlCrN/TiAlYN. High-temperature wear test was conducted on the TiAlCrN/TiAlYN and TiAlCrN coatings using a reciprocating sliding ball-on-disk configuration, [32]. The test conditions were as follows: counterpart, 10 mm diameter hard metal (tungsten carbide) ball, normal load 15 N (initial Hertzian contact pressure 2.1 GPa), reciprocating stroke 2 mm, frequency 15 Hz, test duration 60 minutes, the samples were heated to temperatures of 400, 600, 800 and 900 °C. In this test the two coatings showed very different wear behaviour. For TiAlCrN, increasing the test temperature from 400 °C to 900 °C led to consistent increase of the depth of the wear crater from 0.076 µm to 0.97 µm, whereas the Y-stabilised coating after an initial increase in the wear depth to 1.82 µm at 600 °C showed consistent decrease of the wear depth at higher temperatures, reaching the lowest value of 0.82 µm at 900 °C. Further more the friction coefficient showed similar behaviour, reducing its values from 0.9 at 600 °C to 0.65 at temperatures in the range of 850 – 950 °C. In contrast the TiAlCrN showed consistently high coefficient of friction increasing from 1.1 to 1.6 when the test temperature increased from 600 °C to 900 °C. This peculiar behaviour of the TiAlCrN/TiAlYN can be related to the progressing coating densification (self-healing) with the temperature increase due to the operation of the Y segregation mechanism.

The superior high temperature oxidation and wear resistance of the TiAlCrN/TiAlYN coating have also been demonstrated in a series of high-speed milling trials. Hardened to different hardness steels and different linear cutting speeds between 385 and 500 m·min<sup>-1</sup> have been used to investigate the effect of the cutting temperature on the lifetime of the coated tools.

Depending on the hardness of the work piece and the cutting speed, the measured cutting temperatures ranged from below 700 °C in cutting EN24 steel (HRC 38, cutting speed  $V_c = 385 \text{ m}\cdot\text{min}^{-1}$ ) to 950 °C in cutting hardened A2 steel (HRC 58,  $V_c = 500 \text{ m}\cdot\text{min}^{-1}$ ). The cutting lifetime data of the TiAlCrN/TiAlYN and TiAlCrN coated end mills are presented in Figs. 5a and 5b. In cutting the relatively soft steels EN24 where the cutting temperatures were below 700 °C, the TiAlCrN/TiAlYN had no advantage as compared to the Y-free coating TiAlCrN, Fig. 5a. However, the TiAlCrN/TiAlYN coating had indeed superior performance to the TiAlCrN in cutting harder steels and at higher cutting speeds where the cutting temperatures were above 800 °C. In the extreme case of cutting the A2 steel at cutting speed  $V_c = 500 \text{ m}\cdot\text{min}^{-1}$ , Fig. 5 b, the TiAlCrN/TiAlYN doubled the lifetime of the TiAlCrN.

#### **4. Nanoscale multilayer/superlattice structured TiAlN/VN coatings.**

The excellent wear behaviour of TiAlN/VN in dry sliding conditions has been widely reported elsewhere in [16, 33]. However, the exceptionally low wear rate of  $2.1 \times 10^{-17} \text{ m}^3\text{N}^{-1}\text{m}^{-1}$  is difficult to be explained by the superhardness (42 GPa, [16]) alone or by the distinctive wear mechanism of the superlattice structured coatings, which suggests material removal in 6 – 8 nm thick nano layers as opposed to monolithically grown coatings, where due to severe plastic deformation, bending and cracking of the columns, release of large 50 – 75 nm particles is observed [34]. In the special case, when V is incorporated in the coating constitution, the effect of tribo-oxidation wear mechanism in dry sliding has to be carefully considered. Vanadium is known to form Magnéli-phases with oxygen, with ‘easy’ crystallographic shear planes [35] that can act as solid lubricants in dry sliding conditions. Additionally the low melting point of the  $\text{V}_2\text{O}_5$  ( $T_m = 685 \text{ }^\circ\text{C}$ ), which lies in the range of the flash temperatures achieved at the asperity contacts during sliding, implies friction reduction due to sliding over a molten phase. Cross-sectional TEM analysis of TiAlN/VN coatings of the wear track in pin-on-disk indeed showed formation of a 10-20 nm thick tribo-film, Fig. 6. Raman spectroscopy of the wear debris revealed the presence of  $\text{V}_2\text{O}_5$  [36]. Scanning electron

microscopy (SEM) observations of the wear track after 1 million laps in room temperature pin-on-disk test showed smooth worn surface and almost no transfer of material from the alumina ball used as a counter part [16]. The low friction coefficient of 0.4 measured in this test can be related to the behaviour of the tribo-oxide film containing  $V_2O_5$ . It is believed that the small amount of  $V_2O_5$ , which forms predominantly at the asperity contacts, reduces the coefficient of friction due to melting. The sliding wear mechanism in such conditions resembles very much boundary lubrication, where the surfaces are separated and the junction formation mechanism is suppressed by adsorbed molecular films (in this case molten phase) although appreciable asperity contact may still occur. Thus the synergy between the fine delamination wear mechanism characteristic of superlattice structures and the low melting point of the tribo- film controls the low friction coefficient at room temperature. In the view of potential high temperature applications the oxidation and the tribological behaviour of TiAlN/VN at elevated temperatures have been studied extensively [17, 18, 37]. A combination of differential scanning calorimetry investigations and high temperature (up to 700 °C) tribometry revealed a unique self- adapting behaviour of TiAlN/VN to combined thermal mechanical and chemical wear, [17]. It has been shown that at 700 °C in steady state conditions, low friction coefficient in the range of 0.5 was achieved, Fig. 7, which in effect is similar to the friction coefficient measured at room temperature. To explain this effect an operation of a specific controlling mechanism has been suggested that involves sliding against liquefied oxide scale and conversion of  $V_2O_5$  to lower oxidised Magnéli-phases [17]. The very low value for the coefficient of friction of 0.18 (Fig. 7), measured for the initial stages of the sliding process was related to a sliding over liquefied  $V_2O_5$  phase. A SEM cross section, Fig. 8a, produced through the wear track in TiAlN/VN evidences conclusively the existence of a molten phase during sliding at 700 °C. A smooth surface, with typical features for a solidified layer can be observed. The more detailed view shown in Fig. 8 b, indicates that the melting occurs just for the near- surface region, which also implies that the bulk of the

TiAlN/VN coating remains intact at these temperatures. The second part of the friction curve in Fig. 7 represents the friction behaviour in steady state conditions. The exceptionally low friction coefficient of 0.55 for hard coatings at this temperature range is believed to result from sliding against low shear strength Magnéli-phases of  $V_6O_{13}$  and  $VO_2$  produced by a reduction process of  $V_2O_5$  [38]. The operation of the above- described mechanism however, requires availability of significant amount of  $V_2O_5$  phase, the largest portion of which at 700 °C is produced by thermal oxidation process. Thermo-gravimetric oxidation experiments and isothermal oxidation tests at 550 °C for 30 min showed, that the surface of the TiAlN/VN was almost free of  $V_2O_5$  [18, 37]. Fig. 9a shows an SEM image of the surface after isothermal oxidation at 550 °C. After 30 min exposure, only very thin oxide layer with a needle like morphology has been formed, which did not produce intensive enough signal to be detected by X-ray diffraction. In the temperature range of 500 °C indeed significant increase of the friction coefficient was recorded [17], which implies for the existence of a transition regime in the control mechanisms operating at room and elevated temperatures. At higher temperatures, above 600 °C however, formation of  $V_2O_5$  mixed predominantly with  $AlVO_4$  is detected in sufficient amount to trigger the control mechanism for low friction in steady state conditions. An SEM image of the surface after exposure for 30 min to 638 °C shows that the coating surface was uniformly oxidised, Fig. 9b. A large area of the surface was covered by fine needles/plates, which form with a certain preferred orientation (arrowed). EDX selected area analysis showed that these fine needles/plates were highly V-rich. Further X-ray diffraction analysis confirmed the presence of the  $V_2O_5$  phase. Fig. 10 shows a bright field cross-sectional TEM image of oxide / coating interface region from sample isothermally oxidised at 600 °C for 30 min. The cross section clearly demonstrates that the high temperature did not affect the superlattice structure of the TiAlN/VN below the top oxide layer. The Fresnel contrast from the nanoscale multilayer structure extended right up to the oxide / coating interface, suggesting that no inter- diffusion between the individual layers has taken place.

This observation demonstrates that the bulk of the coating retains the enhanced mechanical properties of the superlattice coatings and the material responds to the environment by adapting its surface properties only. The consistently low and almost identical coefficient of friction recorded for room and 700 °C determine the major application fields for TiAlN/VN, such as protection of wear parts and cutting tools used for machining of softer but much “stickier” materials e.g. Ni based alloys. TiAlN/VN coated 8 mm two flute ball nosed end mills were tested in dry cutting of Inconel 718, HRC43, cutting speed 90 m·min<sup>-1</sup>, axial depth of cut 0.5 mm, feed 0.2 mm. The superlattice coated tools showed the longest length of cut of 380 m, out-performing various PVD coatings: TiAlN, TiAlN+WC/C, TiAlN+MoS<sub>2</sub>, TiAlN+graphite, thus demonstrating the importance of maintaining the low coefficient of friction at elevated temperatures.

## **5. Conclusions**

The experience gained so far in the design, large scale manufacturing and application of nanoscale multilayer/superlattice structured PVD coatings allows us to identify two TiAlN based coatings adapting their tribological properties at high temperatures. In the TiAlCrN/TiAlYN system, high wear resistance and low friction coefficient are achieved due to a segregation mechanism taking place in the bulk of the coating, which results in coating structural densification at high (800 = 950 °C) temperatures. In the TiAlN/VN system, exceptionally low coefficient of friction and wear rates are achieved by the adaptation of the surface properties, due to a compositionally regulated tribo-oxidation process taking place during sliding.

## **Acknowledgements**

This paper has been written as a survey article. The great support of all the Surface Engineering Research Group at the Materials and Engineering Research Institute at Sheffield Hallam University is acknowledged. Parts of the work have been carried out within DTI-Link

Surface Engineering Programme GK/K76351 MULTICOAT and UK Engineering and Physical Science Research Council (EPSRC) Programme, grant No. GR/N23998/01.

## References

- [1] A. A. Voevodin, J. S. Zabinski, *Thin Solid Films* 370 (2000) 223.
- [2] S. Veprek, *J. Vac. Sci. Technol. A*17 (1999) 2401.
- [3] J. Musil, *Surf. Coat. Technol.* 125 (2000) 322.
- [4] R. Hauert, J. Patscheider, *Adv. Eng. Mater.* 2 (2000) 247.
- [5] A. A. Voevodin, J. J. Hu, T. A. Fitz, J. S. Zabinski, *Surf. Coat. Technol.* 146-147 (2001) 351.
- [6] A. Hörling, L. Hultman, M. Odén, J. Sjöln, and L. Karlsson, *J. Vac. Sci. Technol. A*20 (2002) 1815.
- [7] P. H. Mayrhofer, A. Hörling, L. Karlsson, J. Sjöln, C. Mitterer, L. Hultman, *Appl. Phys. Lett.* 83 (2003) 2049.
- [8] M. I. Lembke, D. B. Lewis, W. -D. Münz, J. M. Titchmarsh, *Surf. Eng.* 17 (2001) 153.
- [9] Q. Luo, P. Eh. Hovsepian, D. B. Lewis, W.-D. Münz, Y. N. Kok, J. Cockrem, M. Bolton, A. Farinotti, *Surf. Coat. Technol.* 193 (2005) 219.
- [10] C. Leyens, M. Peters, P. Eh. Hovsepian, D. B. Lewis, Q. Luo, W. -D. Münz, *Surf. Coat. Technol.* 155 (2002) 103.
- [11] D. McIntyre, J. E. Greene, G. Håkansson, J. -E. Sundgren, W. -D. Münz, *J. Appl. Phys.* 67 (1990) 1542.
- [12] I. J. Smith, PhD Thesis, Sheffield Hallam University, UK, 1998.
- [13] A. M. Huntz, in E. Lang (ed.), *The role of Active Elements in the Oxidation of High Temperature Metals and Alloys*, Elsevier Applied Science, London, 1989, p. 81.

- [14] D. P. Moon, *Mater. Sci. Technol.* 5 (1989) 754.
- [15] U. Helmerson, S. Todorova, S. A. Barnett, J.-E. Sundgren, L. C. Markert, J. E. Greene, *J. Appl. Phys.* 62 (1987) 481.
- [16] P. Eh. Hovsepian, D. B. Lewis, W. -D. Münz, *Surf. Coat. Technol.* 133-134 (2000) 166.
- [17] P. H. Mayrhofer, P. Eh. Hovsepian, C. Mitterer, W. -D. Münz, *Surf. Coat. Technol.* 177-178 (2004) 341.
- [18] Z. Zhou, W. M. Rainforth, D. B. Lewis, S. J. Creasey, J. J. Forsyth, F. Clegg, A. P. Ehiasarian, P. Eh. Hovsepian, W. -D. Münz, *Surf. Coat. Technol.* 177-178 (2004) 198.
- [19] W. -D. Münz, D. Schulze, F. J. M. Hauzer, *Surf. Coat. Technol.* 50 (1992) 169.
- [20] W. -D. Münz, C. Schönjahn, H. Paritong, I. J. Smith, *Le Vide*, 55 (2000) 205.
- [21] C. Schönjahn, A. P. Ehiasarian, D. B. Lewis, R. New, W. -D. Münz, *J. Vac. Sci. Technol.* A19 (2001) 1415.
- [22] C. Schönjahn, L. A. Donohue, D. B. Lewis, W. -D. Münz, R. D. Twesten, I. Petrov, *J. Vac. Sci. Technol.* A18 (2000) 1718.
- [23] I. Petrov, P. Losbichler, D. Bergstrom, J. E. Greene, W. -D. Münz, T. Hurkmans, T. Trinh, *Thin Solid Films* 302 (1997) 179.
- [24] M. I. Lembke, D. B. Lewis, W.-D. Münz, *Surf. Coat. Technol.* 125 (2000) 263.
- [25] L. A. Donohue, I. J. Smith, W. -D. Münz, I. Petrov, J. E. Greene, *Surf. Coat. Technol.* 94/95 (1997) 226.
- [26] D. B. Lewis, L. A. Donohue, M. Lembke, W. -D. Münz, R. Kuzel, V. Valvoda, C. Blpomfield, *Surf. Coat. Technol.* 114 (1999) 187.
- [27] S. A. Barnett, *Mechanics and Dielectric Properties*, in *Physics of Thin Films* (Vol. 17), editors M. H. Francombe and J. L. Vossen, Academic Press, Boston, USA, 1993, 2.

- [28] P. Panjan, B. Navinsek, A. Cvelbar, A. Zalar, J. Viecek, Surf. Coat. Technol. 98 (1998)1497.
- [29] H. Oettel, R. Wiedemann. Surf. Coat. Technol. 76-77 (1995) 265.
- [30] M. Lembke, PhD Thesis, Sheffield Hallam University, UK, 2001.
- [31] P. H. Mayrhofer, C. Mitterer, Surf. Coat. Technol 133-134 (2000) 131.
- [32] E. Pflüger, A. Schröer, P. Voumard, L. A. Donohue, W. -D. Münz, Surf. Coat. Technol 115 (1999) 17.
- [33] P. Eh. Hovsepian, W. -D. Münz, Vacuum, 96 (2003) 27.
- [34] Q. Luo, W. M. Rainforth, W. -D. Münz, Wear 74 (1999) 225.
- [35] M. Voydt, A. Skopp, I. Dörfel, K. Vitke, Wear 218 (1998) 84.
- [36] C. P. Constable, J. Yarwood, P. Hovsepian, L. A. Donohue, D. B. Lewis, W. -D. Münz, J. Vac. Sci. Technol. A18 (2000) 1681.
- [37] D. B. Lewis, S. Creasy, Z. Zhou, J.J. Forsyth, A. P. Ehiasarian, P. Eh. Hovsepian, Q. Luo, W. M. Rainforth, W. -D. Münz, Surf. Coat. Technol. 177-178 (2004) 252.
- [38] Y. Niguyi, L. Junuha, L. Chenglu, Appl. Surf. Sci. 191 (2002) 176.

## List of Figure Captions:

Figure 1 Schematic cross sections of (a) the four cathode HTC 1000-4 PVD coating system, and (b) schematic of a typical superlattice structured coating design.

Figure 2 Cross-sectional TEM micrographs of (a) bulk of the TiAlN/CrN superlattice coating, and (b) the base layer region after iso-thermal treatment ( $T = 750\text{ }^{\circ}\text{C}$ , for 1000 h).

Figure 3 Cross-sectional TEM micrograph of TiAlCrN/TiAlYN coating, iso-thermally treated at  $T = 750\text{ }^{\circ}\text{C}$ , for 1000 h.

Figure 4 STEM-EDX maps (a) L-Y and (b)  $K\alpha$ -Y of TiAlCrN/TiAlYN coating, showing segregation of Y at the grain boundaries.

Figure 5 Life-time of 8 mm in diameter two flute ball nosed end mills coated with various coatings (a) in cutting soft EN24 steel (HRC 38) and (b) in cutting hard A2 steel (HRC 58).

Figure 6 Cross-sectional TEM micrograph of TiAlN/VN superlattice coating from the wear track region after pin-on-disk test showing the tribo-film formation.

Figure 7 Friction coefficient curve of TiAlN/VN superlattice coating tested at high temperature of  $700\text{ }^{\circ}\text{C}$  in air atmosphere.

Figure 8 (a) Cross-sectional SEM overview of the wear track on a TiAlN/VN superlattice coating after a tribo-test at  $700\text{ }^{\circ}\text{C}$ , (b) Detailed image of the oxidised coating surface from the indicated area in Fig. 8 a of the wear track.

Figure 9 (a) SEM image from the surface of TiAlN/VN superlattice coating iso-thermally treated at  $T = 550\text{ }^{\circ}\text{C}$ , for 30 minutes; (b) after oxidation in air at  $638\text{ }^{\circ}\text{C}$  for 30 min.

Figure 10 Cross-sectional TEM bright field image of oxide/coating interface region of TiAlN/VN superlattice coating oxidised in air at  $600\text{ }^{\circ}\text{C}$  for 30 min.

Fig. 1

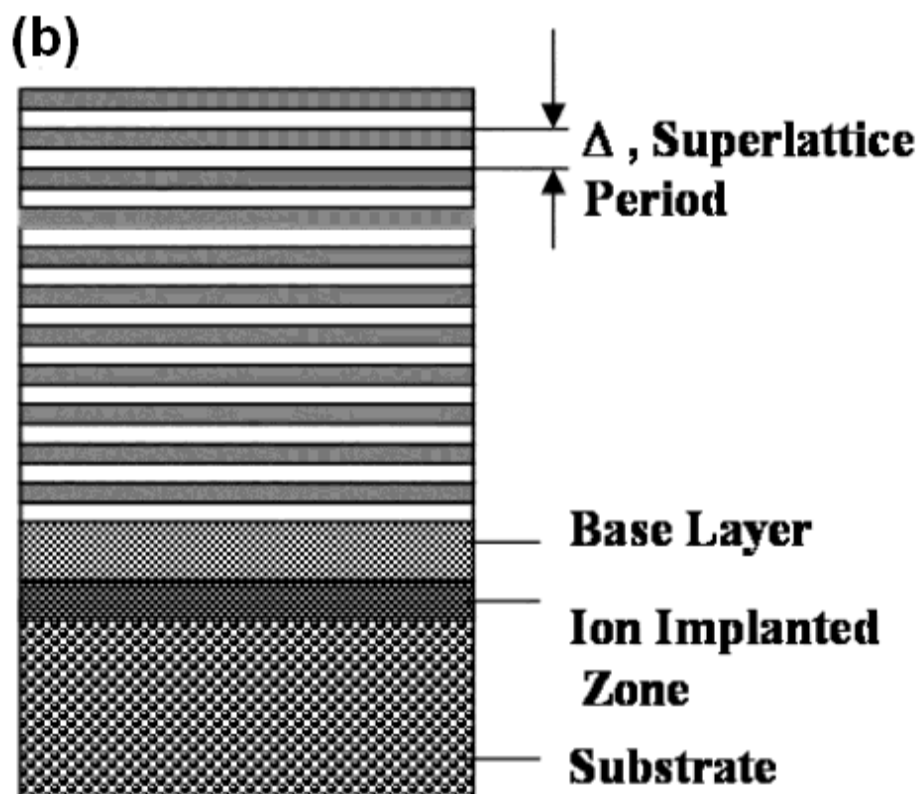
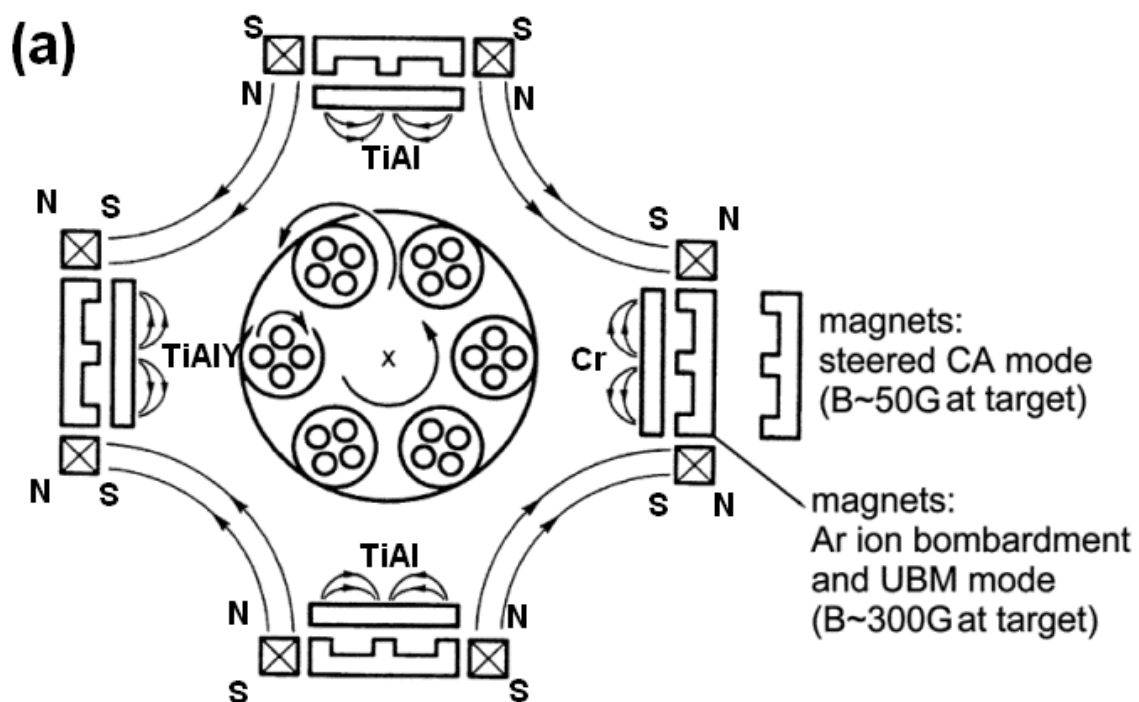


Fig. 2

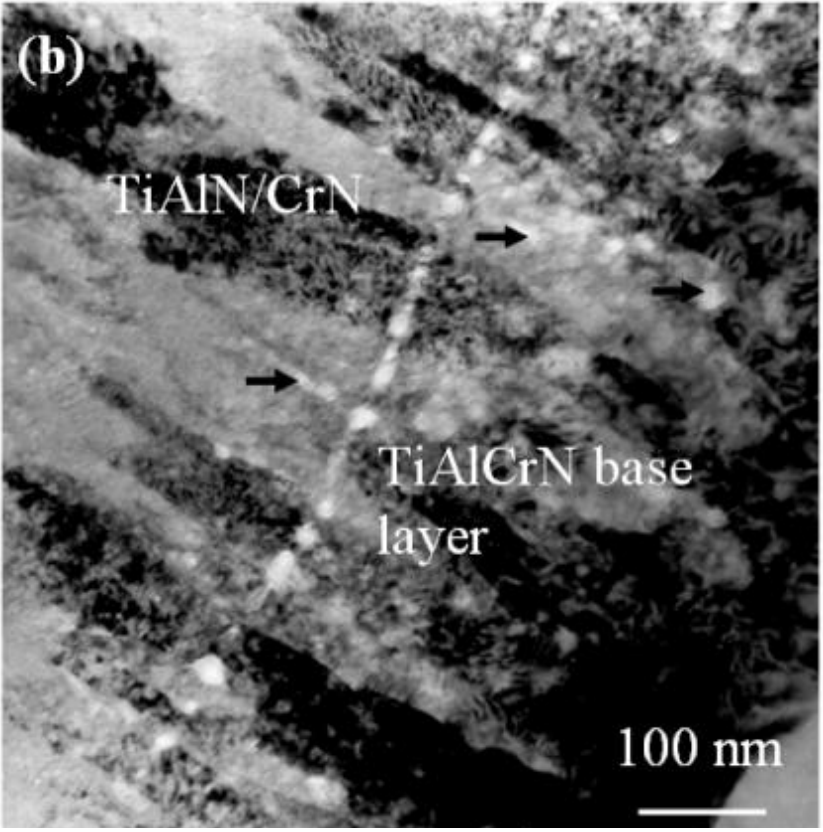
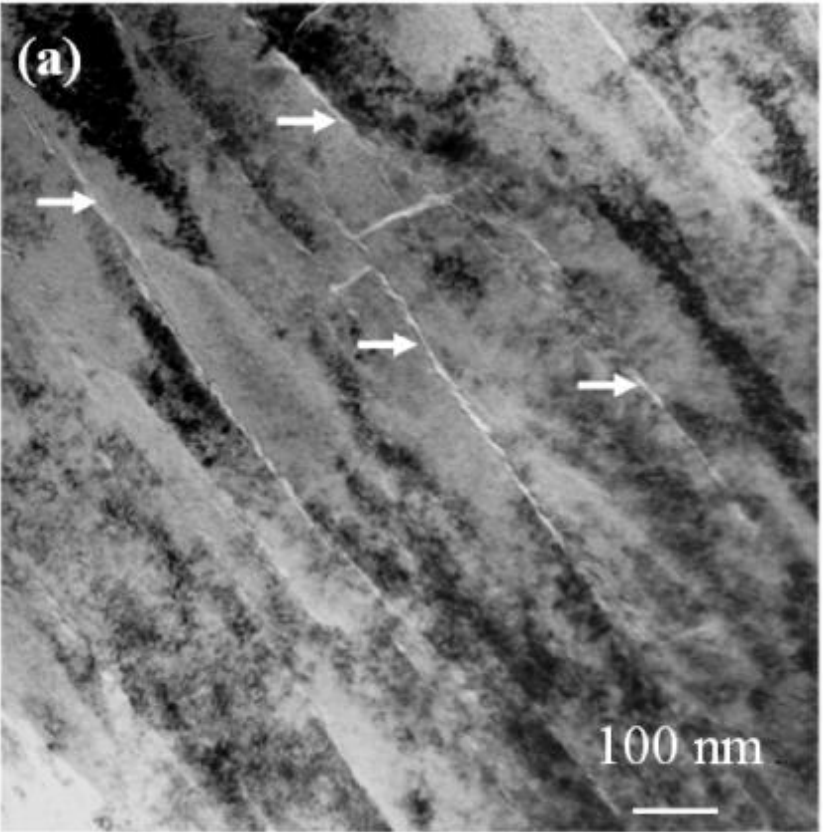
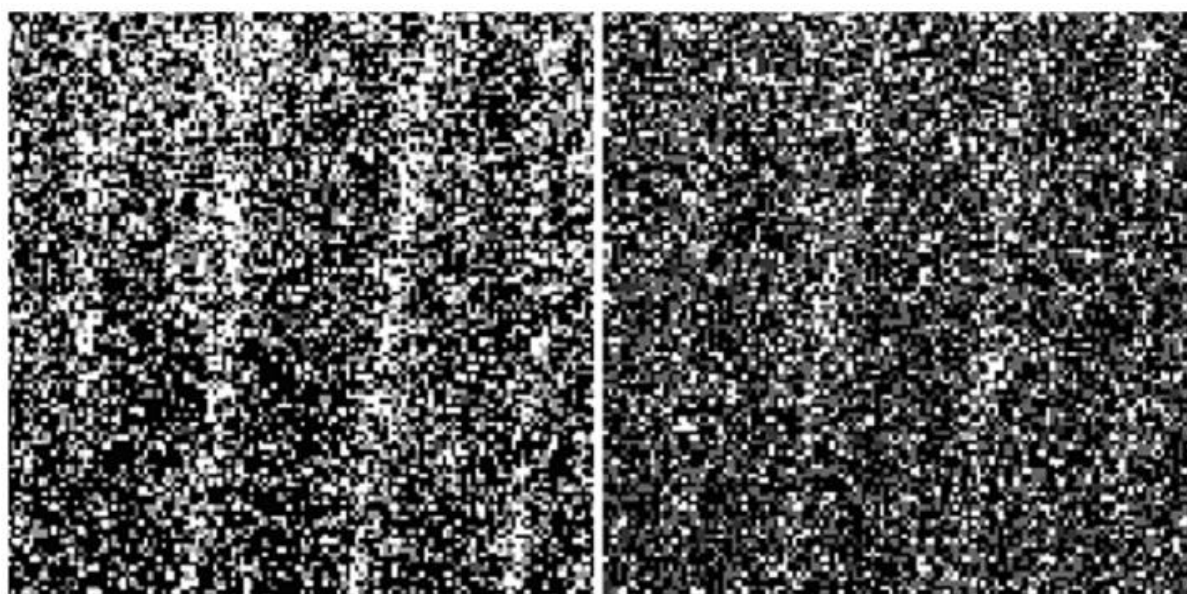


Fig. 3



Fig. 4



(a) L-Y

20 nm

(b) K $\alpha$ -Y

20 nm

Fig. 5

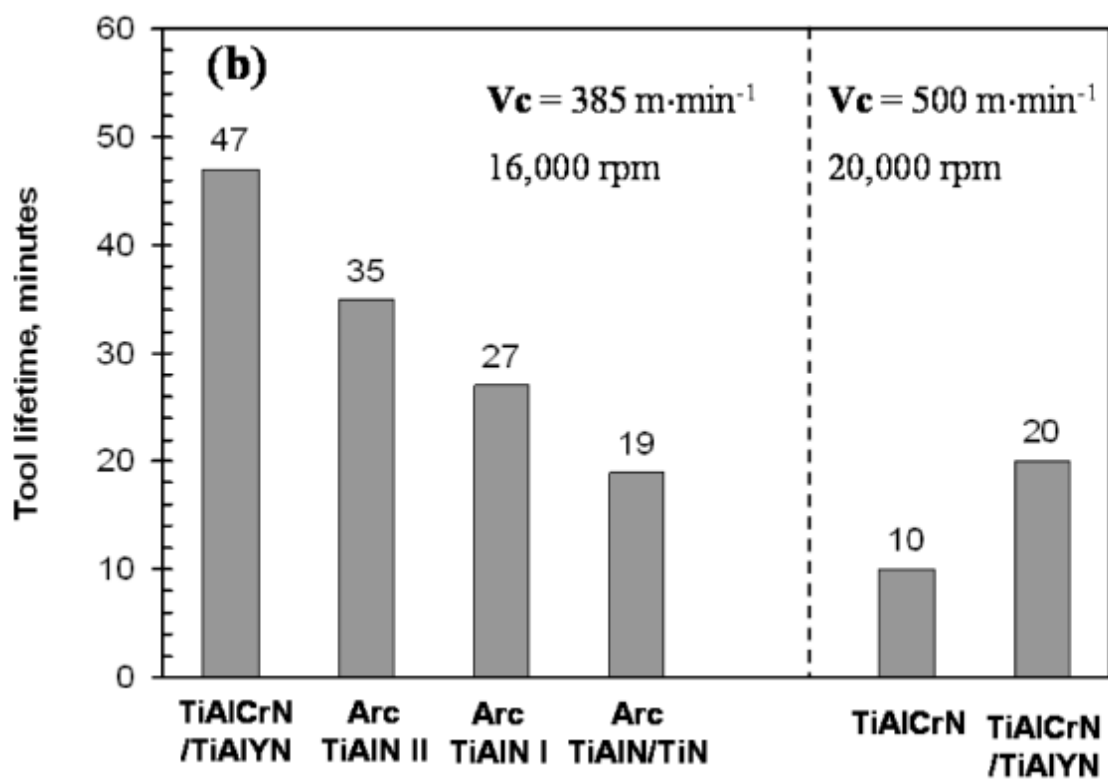
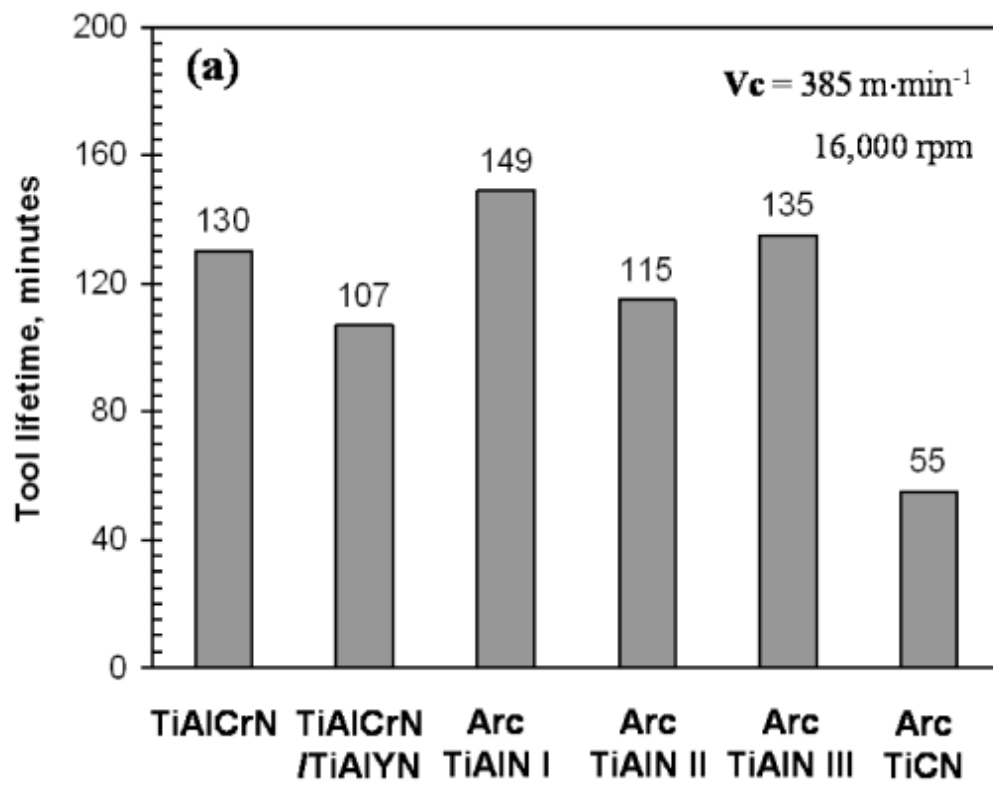


Fig. 6

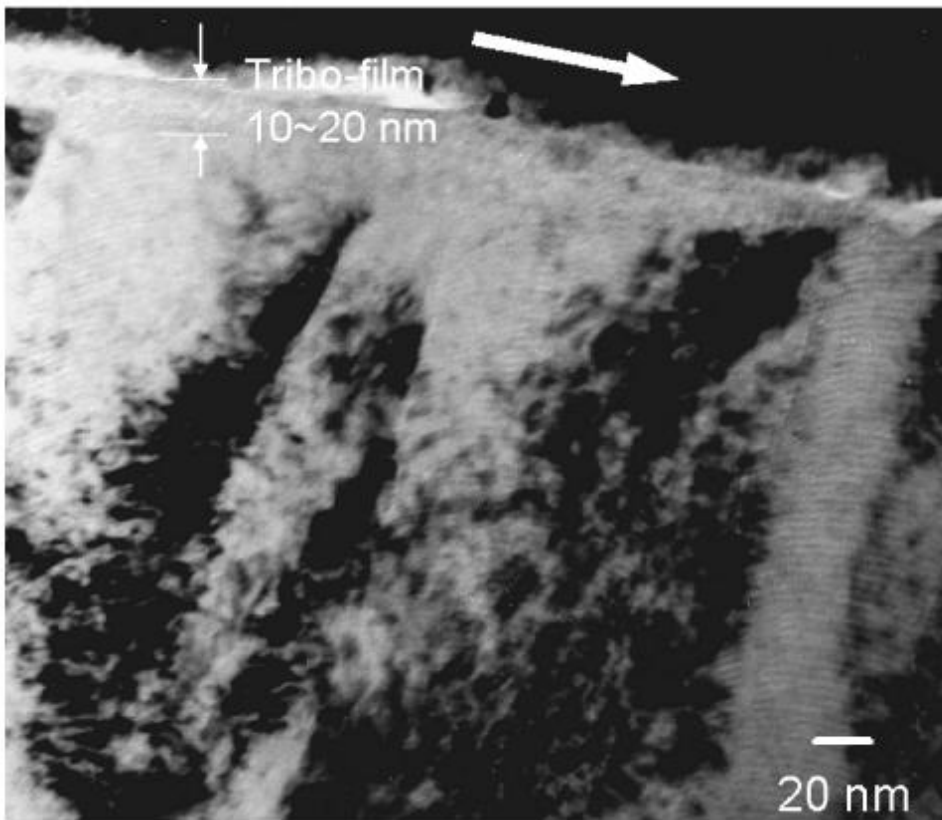


Fig. 7

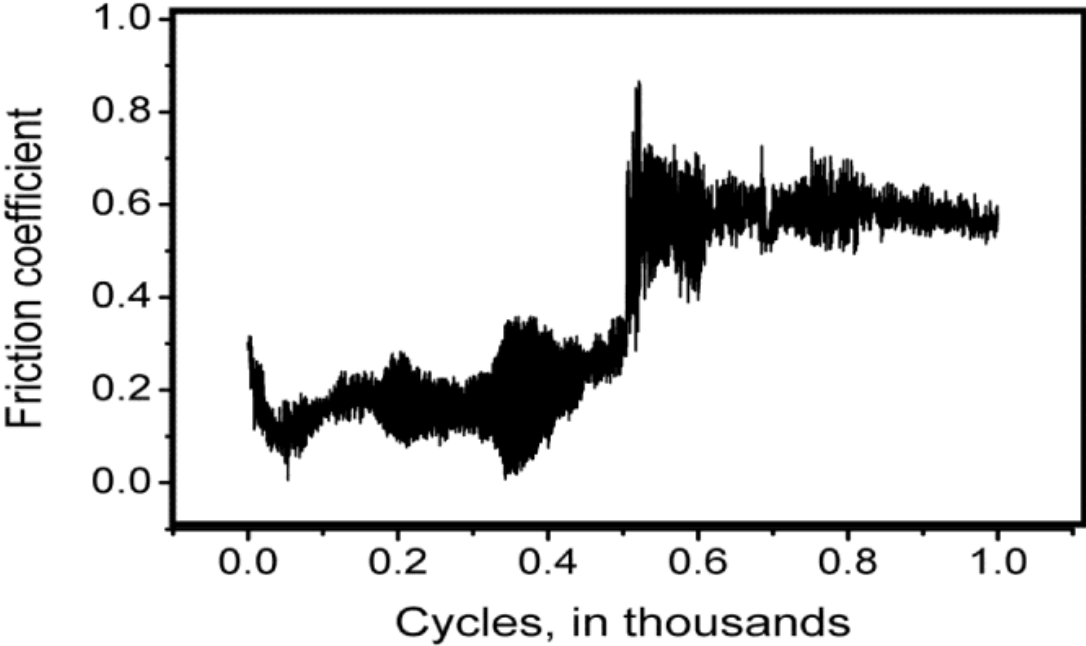


Fig. 8

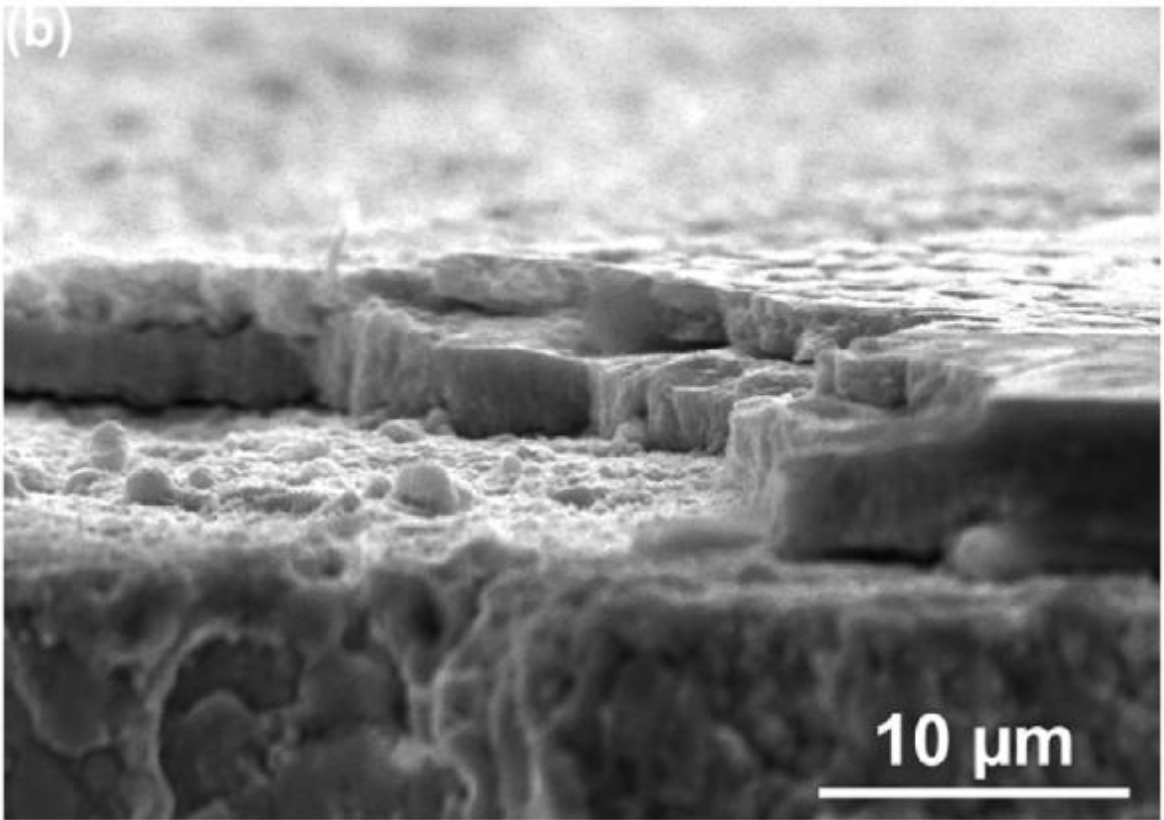
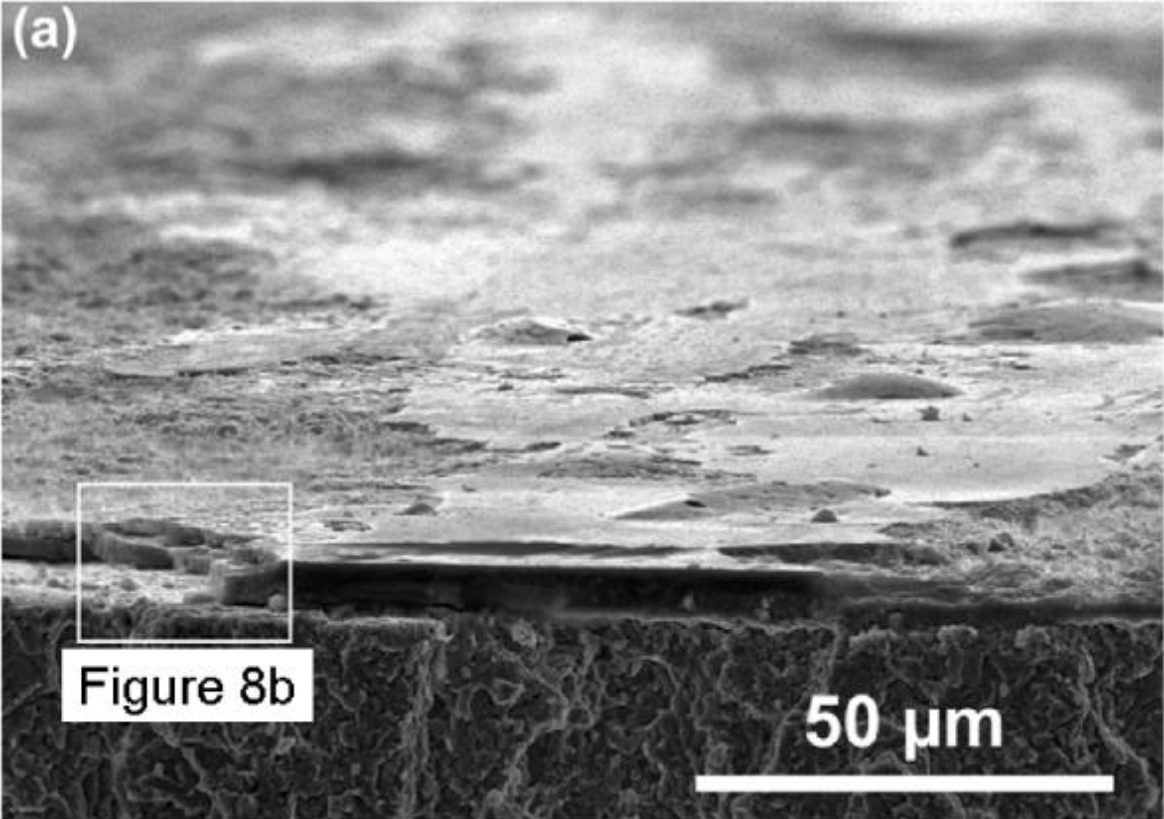


Fig. 9

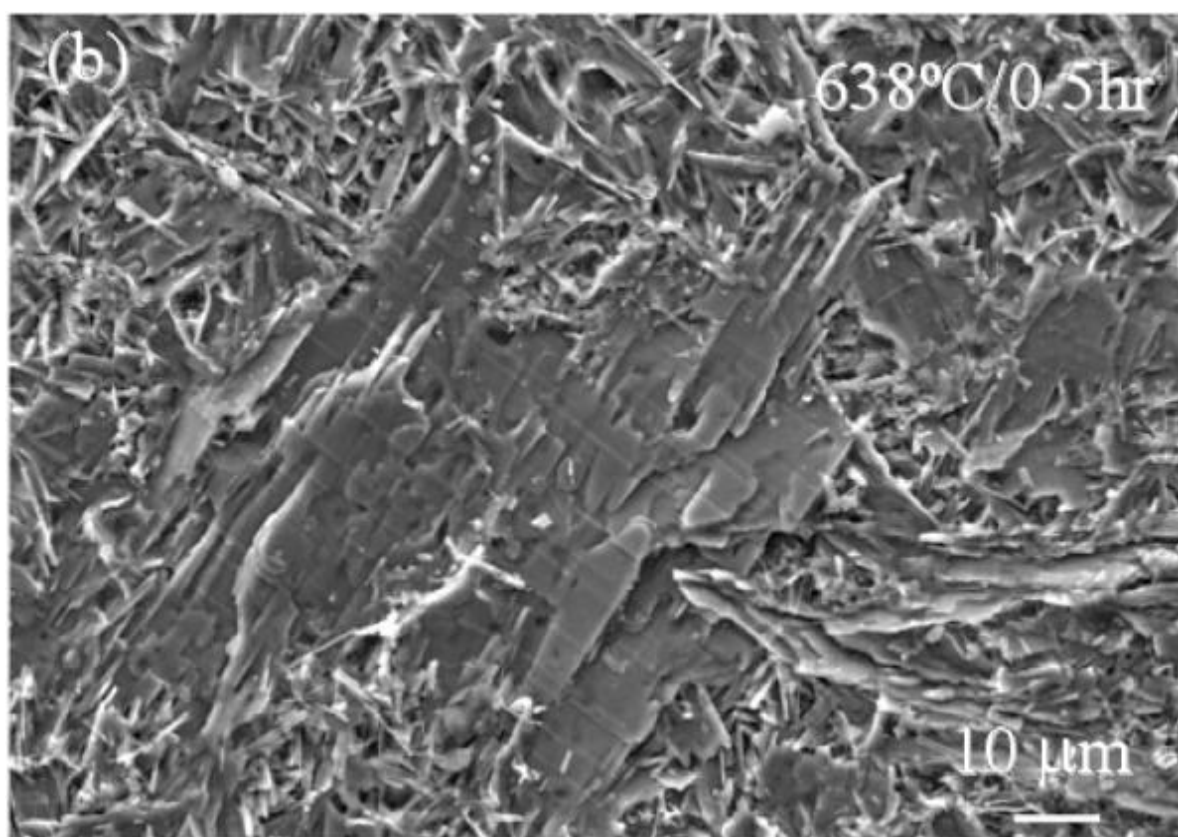
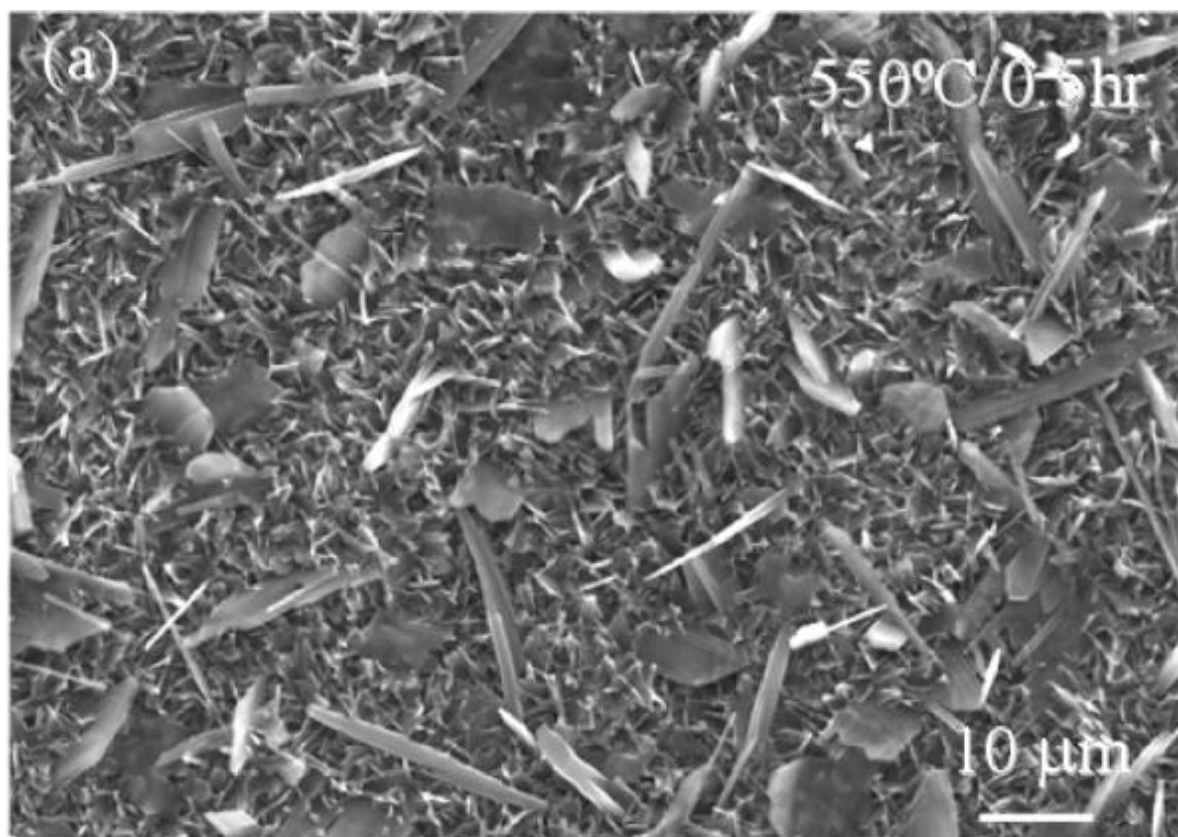


Fig. 10

